
LM-HT SNN: Enhancing the Performance of SNN to ANN Counterpart through Learnable Multi-hierarchical Threshold Model

Zecheng Hao¹, Xinyu Shi^{1,2}, Zhiyu Pan^{1,2}, Yujia Liu¹, Zhaofei Yu^{1,2*} & Tiejun Huang^{1,2*}

¹ School of Computer Science, Peking University

² Institute for Artificial Intelligence, Peking University

Abstract

Compared to traditional Artificial Neural Network (ANN), Spiking Neural Network (SNN) has garnered widespread academic interest for its intrinsic ability to transmit information in a more biological-inspired and energy-efficient manner. However, despite previous efforts to optimize the learning gradients and model structure of SNNs through various methods, SNNs still lag behind ANNs in terms of performance to some extent. The recently proposed multi-threshold model provides more possibilities for further enhancing the learning capability of SNNs. In this paper, we rigorously analyze the relationship among the multi-threshold model, vanilla spiking model and quantized ANNs from a mathematical perspective, then propose a novel LM-HT model, which is an equidistant multi-hierarchical model that can dynamically regulate the global input current and membrane potential leakage on the time dimension. In addition, we note that the direct training algorithm based on the LM-HT model can seamlessly integrate with the traditional ANN-SNN Conversion framework. This novel hybrid learning framework can effectively improve the relatively poor performance of converted SNNs under low time latency. Extensive experimental results have demonstrated that our LM-HT model can significantly outperform previous state-of-the-art works on various types of datasets, which promote SNNs to achieve a brand-new level of performance comparable to quantized ANNs.

1 Introduction

Recognized as the third generation of artificial neural networks [33], Spiking Neural Network (SNN) is increasingly receiving significant academic attention due to its enormous potential in biological plausibility and high energy efficiency. As the information transmission between the pre-synaptic and post-synaptic layers relies on the discrete spike signal, which will be only emitted when the membrane potential of the corresponding neuron exceeds the firing threshold, SNNs have a unique event-driven property compared to conventional Artificial Neural Network (ANN). By utilizing this property, researchers have pointed out that SNNs can achieve significant advantages in terms of energy consumption on neuromorphic hardware [35, 5, 37]. Currently, SNNs have further fulfilled a role in multiple application scenarios including object detection [22], natural language processing [32], and 3D recognition [24].

Spatial-Temporal back-propagation (STBP) with surrogate gradients is currently the most mainstream supervised learning algorithm suitable for SNNs. Although previous works have attempted to further enhance the learning ability of SNNs by delving into various optimization strategies in the field of

*Corresponding authors: yuzf12@pku.edu.cn, tjhuang@pku.edu.cn

STBP training, including gradient adjustment [29, 8, 14] and structural improvement [51, 49, 43], there is still a certain performance gap between ANNs and SNNs.

Recently, the STBP learning algorithm based on multi-threshold models [40, 41] is considered as another potential way to improve the performance of SNNs. In this scenario, multiple levels of the firing threshold enable SNNs to transmit richer information at each time-step. Unfortunately, we think that current related works have not accurately recognized the mathematical essence of multi-threshold models as well as their relationship with ANNs and SNNs. In this paper, we innovatively propose a learnable multi-hierarchical and equidistant threshold model based on global input information, which is called LM-HT model. On the one hand, we note that our LM-HT model can equivalently represent the information of the vanilla model over multiple consecutive time-steps at a single step. Meanwhile, we can regulate the uniformity of the spike sequence by adopting different threshold levels. On the other hand, the STBP method based on the LM-HT model can be transformed into the training modes of the vanilla STBP and quantized ANNs under different parameter initialization conditions, respectively. The main contribution of this work has been summarized as follows:

- We point out that the essence of the equidistant multi-threshold model is to simulate the spike firing situation of the vanilla spiking model within specific time windows that satisfy the condition of uniform input current. Specially, when the input current follows a completely uniform distribution on the time dimension, for the multi-threshold model with a specific parameter setting, the sum of firing spikes is mathematically equivalent to the activation output of quantized ANNs.
- We propose an advanced LM-HT model, which can enhance the performance of SNNs to the level of ANNs while maintaining the basic characteristics of spiking neurons. By adopting different parameter initialization schemes, the LM-HT model can further establish a bridge between the vanilla STBP and quantized ANNs training.
- We further design a brand-new hybrid training framework based on the LM-HT model, which is enable to effectively improve the performance degradation problem of traditional ANN-SNN Conversion methods regardless of the time latency degree involved.
- Experimental results have indicated that our model can fulfill state-of-the-art learning performance for various types of datasets, which demonstrates the superiority of our proposed scheme compared to previous works. For instance, we achieve the top-1 accuracy of 81.76% for CIFAR-100, Resnet-19 within merely 2 time-steps.

2 Related Works

STBP supervised training. STBP is the most prevailing recurrent-mode learning algorithm in the field of SNN direct training. [46] tackled the non-differentiable problem existed in the spike firing process by utilizing surrogate gradients and achieved gradient smoothing calculation between layers. [8] and [14] respectively proposed brand-new target loss functions by analyzing the temporal distribution of the spike sequence and membrane potential. Furthermore, various novel temporal-dependent batch normalization layers [51, 10, 15] and advanced spiking neuron models [49, 43] have been pointed out, which enhances the capability and stability of SNN learning. The researchers also designed a variety of residual blocks [11, 20] and Transformer structures [52, 48] suitable for SNNs, promoting the development of STBP training towards the domains of deep and large-scale models. In addition, some variant and extended learning methods based on STBP have also received widespread attention. Temporal Coding [36] and Time-to-First-Spike (TTFS) [21] algorithm conduct one-time back-propagation based on the specific firing moment, which effectively reduces the training time cost while preserving temporal characteristics. [34] introduced the idea of online learning into vanilla STBP algorithm, which significantly saves training memory overhead by eliminating the gradient chains between different time-steps.

ANN-SNN Conversion. ANN-SNN Conversion is another widely used method for obtaining high-performance SNNs with limited computational resources, which establishes a mathematical mapping relationship between bounded quantization activation functions and the Integrate-and-Fire (IF) models. [3] first proposed a two-step conversion learning framework, which replaces the activation functions of pre-trained ANNs with the IF models layer by layer. On this basis, [16] and [28] classified and summarized the relevant errors existed in the conversion process. [7] and [2] further reduced the conversion errors under the uniform input condition through deriving the optimal values for the bias

term and initial membrane potential. For the critical conversion error caused by uneven spike firing sequences, multiple optimization strategies have been proposed successively, including memorizing the residual membrane potential [17], firing negative spikes [42, 25] and calibrating the offset spikes [18]. In addition, [44] adopted STBP training to finetune the converted SNNs, which further enhances the performance of the conversion series method under low time latency. Currently, ANN-SNN Conversion has been further applied to the training of large-scale visual and language models [45, 32].

Spiking neural models with multi-threshold. The current proposed multi-threshold spiking neuron models can be generally divided into two types: one emits signed spikes [22, 50, 42], while the other emits multi-bit spikes [27, 40, 41, 24]. However, most of these works consider using multi-threshold models to reduce the conversion errors existed in the ANN-SNN Conversion process, or adopting the hard-reset mechanism which will cause a potential information loss about residual membrane potential, while the rest are limited by relatively small data scale. In this paper, we have the foresight to recognize the mathematical equivalence relationship between equidistant multi-threshold models and quantized ANNs under the conditions of using the soft-reset mechanism and uniform input current, achieving the current optimal performance of SNNs in the domain of STBP learning.

3 Preliminaries

The spiking neuron models for SNNs. The Leaky-Integrate-and-Fire (LIF) model is one of the most commonly used spiking neuron models in the current SNN community. The following equations have depicted the dynamic procedure of the LIF model in a discrete form:

$$\mathbf{m}_{LIF}^l(t) = \lambda_{LIF}^l \mathbf{v}_{LIF}^l(t-1) + \mathbf{I}^l(t) \quad (1)$$

$$\mathbf{v}_{LIF}^l(t) = \mathbf{m}_{LIF}^l(t) - \mathbf{s}_{LIF}^l(t)\theta^l, \quad (2)$$

$$\mathbf{I}^l(t) = \mathbf{W}^l \mathbf{s}_{LIF}^{l-1}(t)\theta^{l-1}, \quad (3)$$

$$\mathbf{s}_{LIF}^l(t) = \begin{cases} 1, & \mathbf{m}_{LIF}^l(t) \geq \theta^l \\ 0, & \text{otherwise} \end{cases}. \quad (4)$$

Eq.(1) describes the charging process of the LIF model: $\forall t \in [1, T]$, $\mathbf{m}_{LIF}^l(t)$ and $\mathbf{v}_{LIF}^l(t-1)$ respectively represent the membrane potential before and after the charging at the t -th time-step. $\mathbf{I}^l(t)$ denotes the input current and λ^l characterizes the leakage degree of the membrane potential. When $\lambda_{LIF}^l = 1$, the LIF model will degenerate into a more specialized model called the IF model. Eq.(2) depicts the reset process of the LIF model: $\mathbf{s}_{LIF}^l(t)$ indicates the spike emitting situation and θ^l is the firing threshold. Here we adopt the soft-reset mechanism, which means that the reset amplitude of the membrane potential is equal to the value of θ^l . Eq.(4) represents the firing process: the model chooses to emit a spike only when the membrane potential after charging has exceeded the threshold.

The supervised learning algorithm for SNNs. STBP is currently the most mainstream learning method. The gradient calculation mode of STBP is inspired by the back-propagation Through Time (BPTT) algorithm in Recurrent Neural Network (RNN), which will propagate along the spatial and temporal dimensions of SNNs simultaneously. Following equations have described the specific propagation process of the STBP algorithm:

$$\frac{\partial \mathcal{L}}{\partial \mathbf{m}_{LIF}^l(t-1)} = \underbrace{\frac{\partial \mathcal{L}}{\partial \mathbf{s}_{LIF}^l(t-1)} \frac{\partial \mathbf{s}_{LIF}^l(t-1)}{\partial \mathbf{m}_{LIF}^l(t-1)}}_{\text{spatial dimension}} + \underbrace{\frac{\partial \mathcal{L}}{\partial \mathbf{m}_{LIF}^l(t)} \frac{\partial \mathbf{m}_{LIF}^l(t)}{\partial \mathbf{v}_{LIF}^l(t-1)} \frac{\partial \mathbf{v}_{LIF}^l(t-1)}{\partial \mathbf{m}_{LIF}^l(t-1)}}_{\text{temporal dimension}}, \quad (5)$$

$$\frac{\partial \mathbf{s}_{LIF}^l(t)}{\partial \mathbf{m}_{LIF}^l(t)} = \text{sign} \left(\left| \mathbf{m}_{LIF}^l(t) - \theta^l \right| \leq \frac{\theta^l}{2} \right). \quad (6)$$

Here \mathcal{L} denotes the target loss function. From Eq.(4) we can note that the mathematical relationship between $\mathbf{s}_{LIF}^l(t)$ and $\mathbf{m}_{LIF}^l(t)$ is equivalent to $\mathbf{s}_{LIF}^l(t) = H(\mathbf{m}_{LIF}^l(t) - \theta^l)$, where $H(\cdot)$ denotes Heaviside step function. As Heaviside function is non-differentiable, researchers consider using a surrogate function, which is approximate to Heaviside function but differentiable, to handle the term $\frac{\partial \mathbf{s}_{LIF}^l(t)}{\partial \mathbf{m}_{LIF}^l(t)}$ in the back-propagation chain. Eq.(6) describes the well-known rectangular surrogate function.

Quantized ANNs. The quantized ANN model is a widely used structure in the field of ANN-SNN Conversion. Compared to traditional ANNs, quantized ANNs usually use the following Quantization-Clip-Floor-Shift (QCFS) function [28, 2] as their activation function:

$$\mathbf{a}^l = \frac{\vartheta^l}{T_q} \text{clip} \left(\left\lfloor \frac{\mathbf{W}^l \mathbf{a}^{l-1} T_q + \varphi^l}{\vartheta^l} \right\rfloor, 0, T_q \right). \quad (7)$$

Here \mathbf{a}^l and φ^l represent the activation output and shift factor on the l -th layer of the quantized ANN, respectively. T_q and ϑ^l denote the quantization level and learnable scaling factor. If we set $T_q = T$, $\vartheta^l = \theta^l$, $\mathbf{a}^l = \sum_{t=1}^T \mathbf{s}_{IF}^l(t) \theta^l / T$, $\mathbf{v}_{IF}^l(0) = \varphi^l$, one can find that the so-called QCFS function actually simulate the average spike firing rate of the IF model (we set $\mathbf{r}_{IF}^l(T_q) = \sum_{t=1}^{T_q} \mathbf{s}_{IF}^l(t) \theta^l / T_q$) under the condition of the uniform input current and soft-reset mechanism (the detailed discussion will be provided in the following text). This conclusion suggests that SNNs have the potential to maintain the same level of performance as ANNs under specific conditions.

4 Methodology

4.1 The Multi-hierarchical Threshold (M-HT) Model

In this section, we first introduce the M-HT model, which is an advanced spiking neural model with multi-hierarchical firing threshold. The M-HT model has equidistant multi-level thresholds and will select the threshold closest to its current membrane potential at each time-step to achieve the process of firing spikes and resetting potential. Eqs. (8)-(11) describe the dynamic equations of the M-HT model.

$$\mathbf{m}^l(t) = \lambda^l \mathbf{v}^l(t-1) + \mathbf{I}^l(t), \quad (8)$$

$$\mathbf{v}^l(t) = \mathbf{m}^l(t) - \mathbf{s}^l(t) \theta^l, \quad (9)$$

$$\mathbf{I}^l(t) = \mathbf{W}^l \mathbf{s}^{l-1}(t) \theta^{l-1}, \quad (10)$$

$$\mathbf{s}^l(t) = \begin{cases} L, & \mathbf{m}^l(t) \geq L\theta^l \\ k, & k\theta^l \leq \mathbf{m}^l(t) < (k+1)\theta^l, k = 1, \dots, L-1 \\ 0, & \text{otherwise} \end{cases} \quad (11)$$

Here L denotes the number of level for the firing threshold. As the M-HT model has L different spike firing options at each time-step, we can consider the information transmitted by the M-HT model at one time-step as the information integration of the vanilla neuron model for L time-steps. Therefore, we attempt to bridge a mathematical equivalent relationship between the M-HT and IF model and draw the following conclusion for the M-HT model at any single time-step.

Lemma 4.1. $\forall t \in [1, T]$, if $\mathbf{v}^l(t-1) \in [0, \theta^l)$, the effect of inputting current $\mathbf{I}^l(t)$ into a M-HT model with L -level threshold at the t -th time-step, is equivalent to continuously inputting uniform current $\mathbf{I}^l(t)/L$ for L time-steps into a IF model with $\mathbf{v}_{IF}^l(0) = \mathbf{v}^l(t-1)$, i.e. $\mathbf{s}^l(t) = \text{clip} \left(\left\lfloor \frac{\mathbf{v}^l(t-1) + \mathbf{I}^l(t)}{\theta^l} \right\rfloor, 0, L \right) = \sum_{j=1}^L \mathbf{s}_{IF}^l(j)$.

Lemma 4.1 indicates that the M-HT model under a single time-step can be used to simulate the total number of spikes emitted by the IF model under uniform input current within L consecutive time-steps. Regarding the surrogate gradient calculation of the M-HT model, similar to the vanilla spiking models, we propose $\frac{\mathbf{s}^l(t)}{\mathbf{m}^l(t)} = \text{sign} \left(\frac{1}{2}\theta^l \leq \mathbf{m}^l(t) \leq (L + \frac{1}{2})\theta^l \right)$, which covers a wider range of the membrane potential, as shown in Fig.1(d)-(e). Note that $\mathbf{s}(t)$ in Lemma 4.1 can also be calculated through $\text{clip}(\lfloor \cdot \rfloor, \cdot, \cdot)$, which is very similar to the QCFS function mentioned before in quantized ANNs. Furthermore, the back-propagation gradient of QCFS function is usually calculated with ClipReLU function, which is also consistent with the surrogate gradient function of the M-HT model mentioned before. The above analysis preliminarily demonstrates that the M-HT model can achieve the same-level performance as pre-trained ANNs with L -level quantization under single-step condition.

4.2 The Representation Ability of the M-HT Model on Multiple Time-steps

Based on Lemma 4.1, we further consider the information representation of the M-HT model on multiple time-steps and derive the following theorem:

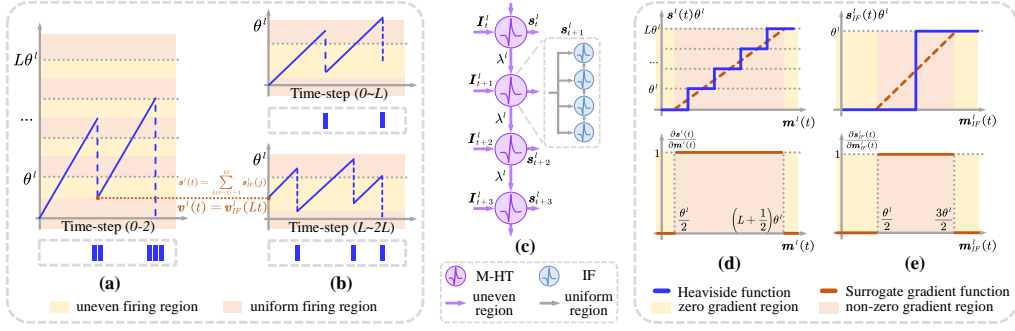


Figure 1: Forward and backward propagation of the M-HT model. (a)-(c): mathematical relationship between the M-HT model and vanilla IF model. (d)-(e): surrogate gradient calculation for the M-HT model.

Theorem 4.2. When $\lambda^l = 1$, $v^l(0) \in [0, \theta^l)$, for a M-HT model with L -level threshold, after T time-steps, we will derive the following conclusions:

(i) If we further assume $\forall t \in [1, T], I^l(t) \in [0, L\theta^l)$, we will have: $\forall t \in [1, T], s^l(t) = \sum_{j=L(t-1)+1}^{Lt} s_{IF}^l(j)$, $v^l(t) = v_{IF}^l(Lt)$, $\sum_{t=1}^T s^l(t) = \sum_{j=1}^{LT} s_{IF}^l(j)$.

(ii) If we further assume $I^l(1) = \dots = I^l(T)$, we will have: $\sum_{t=1}^T s^l(t) = \text{clip} \left(\left\lfloor \frac{v^l(0) + \sum_{t=1}^T I^l(t)}{\theta^l} \right\rfloor, 0, LT \right)$.

Here the IF model has uniform input currents $I^l(1)/L, \dots, I^l(T)/L$ respectively within every L steps and satisfies $v_{IF}^l(0) = v^l(0)$.

The proofs of Lemma 4.1 and Theorem 4.2 have been provided in the Appendix. From Theorem 4.2(i) and Fig.1(a)-(c), one can find that the M-HT model is actually equivalent to dividing the spike firing sequence of the IF model on consecutive LT steps into T L -step time windows. Combining with the soft-reset mechanism, the M-HT model actually focuses on a specific time window of the vanilla IF model at each time-step and maintains an equal membrane potential with the IF model at the end of each time window (i.e. $\forall t \in [1, T], v^l(t) = v_{IF}^l(Lt)$). The M-HT model follows the assumption of uniform input current within each window and different input currents can be chosen for different windows. In addition, membrane potential leakage can also be adopted between windows.

Overall, the M-HT model can represent the spike firing rate of the IF model within LT time-steps, while maintaining the basic biological characteristics of spiking neurons between different time-steps. When the input current of the M-HT model follows a complete uniform distribution on the time dimension, according to Theorem 4.2(ii), the M-HT model can further simulate the output of an ANN with LT -level quantization layer by layer.

4.3 The Learnable Multi-hierarchical Threshold (LM-HT) Model

The uniform and uneven firing regions in the M-HT model. For a specific number of firing spikes, the M-HT model can often provide multiple spike firing sequences. For example, $[1, 1]$, $[0, 2]$, $[2, 0]$ can all represent the situation where 2 spikes are emitted with 2 time-steps. Here we consider $[1, 1]$ as a case of uniform firing situation, while $[0, 2]$, $[2, 0]$ are viewed as uneven firing situations. However, even when the input current is uniformly distributed, as the sum of spikes in $[0, LT]$ that cannot be divided by L is unable to be represented by a uniform spike output sequence, there are still uneven firing situations:

Corollary 4.3. If $\lambda^l = 1$, $v^l(0) = 0$ and $I^l(1) = \dots = I^l(T)$, for a M-HT model with L -level threshold, $s^l(1) = \dots = s^l(T)$ is only satisfied when $I^l(1) \in [k\theta^l, k\theta^l + \theta^l/T), \forall k = 0, \dots, L-1$ or $I^l(1) \in (-\infty, 0) \cup [L\theta^l, +\infty)$.

The proof of Corollary 4.3 is provided in the Appendix. From Corollary 4.3, we can divide the input current into uniform and uneven firing regions according to the corresponding intervals, as shown

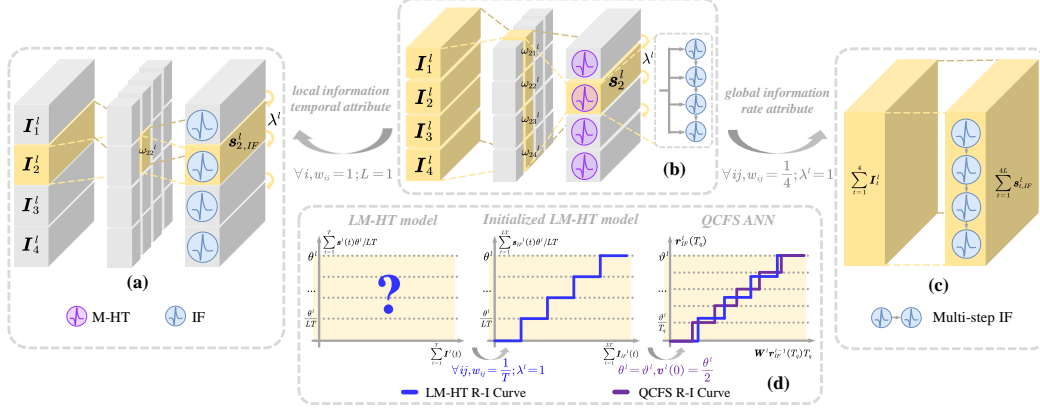


Figure 2: The STBP learning framework based on the LM-HT model. (a): vanilla STBP training. (b): STBP training with the LM-HT model. (c): direct training of quantized ANNs. (d): hybrid training with the LM-HT model, here R-I Curve denotes Rate-Input Curve.

in Fig.1(a)-(b). Note that the uneven spike sequences emitted by the l -th layer may further cause the input current of the $l + 1$ -th layer to no longer meet the precondition of uniform distribution mentioned in Corollary 4.3, and then the output spike sequences corresponding to the sum of spikes divisible by L may also become uneven for the $l + 1$ -th layer. That is to say, as the number of layers increases, the area of the uneven firing regions will tend to expand gradually if we do not manually homogenize the input current layer by layer.

Learnable Temporal-Global Information Matrix and membrane leaky parameters. Enhancing the uniform spike firing pattern can promote the MH-T model to achieve superior performance similar to quantized ANNs, while uneven spike sequences retain more temporal information and biological characteristics of SNNs. Therefore, how to comprehensively utilize these two spike firing patterns has become a critical problem. To address this issue, inspired by [12], we first introduce the concept of Temporal-Global Information Matrix (T-GIM):

$$\forall t \in [1, T], \mathbf{I}^l(t) = \sum_{j=1}^T \omega_{tj}^l \mathbf{W}^l \mathbf{s}^{l-1}(j) \theta^{l-1}. \quad (12)$$

Here ω_{tj}^l is the element at row t and column j of the T-GIM $\mathbf{\Omega}^l$, $\mathbf{\Omega}^l \in \mathbb{R}^{T \times T}$. After using T-GIM, the input current will be calculated by Eq.(12). At this point, this brand-new input current adopts a multi-step current weighting form, allowing the model to simultaneously focus on the global information along the time dimension at each-step, as shown in Fig.2(b). Note that the new input current will follow a uniform distribution when $\forall i, j \in [1, T], \omega_{ij}^l = \frac{1}{T}$ and degrade to the vanilla input current when $\mathbf{\Omega}^l = \text{diag}(1, \dots, 1)$. For the first case mentioned above, if we further add the condition $\lambda^l = 1$, according to Theorem 4.2(ii), one can find that the output of the model will be consistent with the activation output of a LT -level quantized ANN layer by layer, as shown in Fig.2(b)-(c). For the second case, when $L = 1$, the model will degenerate into vanilla LIF model, as shown in Fig.2(a)-(b).

To enable the model to dynamically adjust the above calculation process, we set both $\mathbf{\Omega}^l$ and λ^l as learnable parameters. The initial values of $\mathbf{\Omega}^l$ and λ^l are set to $1/T$ and 1, respectively. During the training process, we choose the Sigmoid function $\sigma(\cdot)$ to control the parameters for fulfilling smooth gradient updates within a bounded learning range. We call this novel model as Learnable Multi-hierarchical Threshold (LM-HT) Model, which combines T-GIM and learnable attributes. We think the LM-HT model can regulate its spike firing pattern more flexibly and reasonably.

Since we can regulate the computational relationships between different time-steps through learnable $\mathbf{\Omega}^l$ and λ^l in the LM-HT model, during the back-propagation process, unlike Eq.(5), we detach the term $\frac{\partial \mathcal{L}}{\partial \mathbf{m}^l(t)} \frac{\partial \mathbf{m}^l(t)}{\partial \mathbf{v}^l(t-1)} \frac{\partial \mathbf{v}^l(t-1)}{\partial \mathbf{m}^l(t-1)}$ from the gradient calculation graph, thereby reducing redundant calculations and completely leaving the gradient propagation between different time-steps to $\mathbf{\Omega}^l$ and λ^l for control. The back-propagation calculation chains for the LM-HT model have been described

as follow. Here \odot denotes the Hadamard product.

$$\frac{\partial \mathcal{L}}{\partial \mathbf{m}^l(t)} = \frac{\partial \mathcal{L}}{\partial \mathbf{s}^l(t)} \frac{\partial \mathbf{s}^l(t)}{\partial \mathbf{m}^l(t)}, \quad (13)$$

$$\frac{\partial \mathcal{L}}{\partial \lambda^l} = \sum_{t=1}^T \frac{\partial \mathcal{L}}{\partial \mathbf{m}^l(t)} \odot \mathbf{v}^l(t-1), \quad (14)$$

$$\frac{\partial \mathcal{L}}{\partial \omega_{ij}^l} = \frac{\partial \mathcal{L}}{\partial \mathbf{m}^l(i)} \odot (\mathbf{W}^l \mathbf{s}^{l-1}(j) \theta^{l-1}), \quad (15)$$

$$\frac{\partial \mathbf{s}^l(t)}{\partial \mathbf{m}^l(t)} = \text{sign} \left(\frac{1}{2} \theta^l \leq \mathbf{m}^l(t) \leq \left(L + \frac{1}{2} \right) \theta^l \right). \quad (16)$$

4.4 Hybrid Training based on the LM-HT Model

Although the traditional ANN-SNN Conversion frameworks have much lower computational overhead than STBP training algorithm, a serious performance degradation phenomenon often exists on the converted SNNs under low time latency [17]. To address this problem, previous researchers [38] considered adopting STBP training for a few epochs on the pre-trained ANN models to enhance the performance of the converted SNNs under fewer time-steps, which is called as hybrid training. In this work, we propose a brand-new hybrid training framework based on the LM-HT model.

We firstly choose QCFS function to train the quantized ANN models and then replace the QCFS function modules layer by layer with the LM-HT models under specific initialization ($\forall i, j \in [1, T], \omega_{ij}^l = \frac{1}{T}; \lambda^l = 1, \theta^l = \vartheta^l, \mathbf{v}^l(0) = \frac{\theta^l}{2}$), as shown in Fig.2(d). Combining with the conclusion pointed out by [2], one can note that the initialized LM-HT model and the QCFS function before substitution have an equivalence in terms of mathematical expectation, which has been described as the following theorem:

Theorem 4.4. *When $\sum_{t=1}^T \mathbf{I}^l(t)/LT = \mathbf{W}^l \mathbf{r}_{IF}^{l-1}(T_q)$ and $\sum_{t=1}^T \mathbf{I}^l(t) \in [0, LT\theta^l]$, if $\forall i, j \in [1, T], \omega_{ij}^l = \frac{1}{T}$ and $\lambda^l = 1, \theta^l = \vartheta^l, \mathbf{v}^l(0) = \frac{\theta^l}{2}$, for L, T, T_q with arbitrary values, we have: $\mathbb{E} \left(\frac{\sum_{t=1}^T \mathbf{s}^l(t) \theta^l}{LT} - \frac{\vartheta^l}{T_q} \text{clip} \left(\left\lfloor \frac{\mathbf{W}^l \mathbf{r}_{IF}^{l-1}(T_q) T_q}{\vartheta^l} + \frac{1}{2} \right\rfloor, 0, T_q \right) \right) = 0$.*

Theorem 4.4 indicates that regardless of whether the time-steps we choose during the STBP training phase is equal to the inference steps simulated in ANN-SNN Conversion, the average spike firing rate of the LM-HT models under the initial state of STBP training maintains a mathematical equivalence with that simulated by the QCFS function modules in the previous stage. Therefore, under this new training framework, we can adopt STBP algorithm to optimize the inference performance of SNN under any degree of time latency. The detailed pseudo-code of our hybrid training algorithm has been provided in the Appendix.

5 Experiments

To validate the effectiveness of our proposed STBP and hybrid training frameworks based on the LM-HT model, we consider multiple static and neuromorphic datasets with different data scale, including CIFAR-10, CIFAR-100 [23], ImageNet-200 [6] and DVSCIFAR-10 [26]. Consistent with the previous works, we also choose VGG [39] and ResNet [19] as the basic network architecture of our model. As the information transmitted by our L -level LM-HT model within T time-steps remains at the same level as that of the vanilla LIF model within LT time-steps, to make a fair evaluation, we will compare the performance of the L -level LM-HT model within T steps with that of the previous works within LT steps.

5.1 Comparison with Previous SoTA Works

We first investigate the competitiveness of our proposed model in the domain of STBP learning. As shown in Table 1, our comparative works incorporate previous state-of-the-art (SoTA) methods in various sub-domains of STBP training, including batchnorm layer optimization [51, 15], improved

Table 1: Comparison with previous state-of-the-art works.

Dataset	Method	Architecture	Time-steps	Accuracy(%)	
CIFAR-10	[51]	STBP-tdBN	ResNet-19	4	92.92
	[29]	Dspike	ResNet-18	4	93.66
	[8]	TET	ResNet-19	4	94.44
	[34]	SLTT	ResNet-18	6	94.44
	[49]	GLIF	ResNet-18	2, 4, 6	94.15, 94.67, 94.88
			ResNet-19	2, 4, 6	94.44, 94.85, 95.03
	Ours (L=2)	LM-HT	ResNet-18	2	96.25
		ResNet-19	2	96.89	
CIFAR-100	[29]	Dspike	ResNet-18	4	73.35
	[8]	TET	ResNet-19	4	74.47
	[34]	SLTT	ResNet-18	6	74.38
	[49]	GLIF	ResNet-18	2, 4, 6	74.60, 76.42, 77.28
			ResNet-19	2, 4, 6	75.48, 77.05, 77.35
	[14]	RMP-Loss	ResNet-19	2, 4, 6	74.66, 78.28, 78.98
	Ours (L=2)	LM-HT	ResNet-18	2	79.33
		ResNet-19	2	81.76	
ImageNet-200	[13]	DCT	VGG-13	125	56.90
	[47]	Online-LTL	VGG-13	16	54.82
		Offline-LTL	VGG-13	16	55.37
	[43]	ASGL	VGG-13	4, 8	56.57, 56.81
	Ours (L=2)	LM-HT	VGG-13	2	61.04
	Ours (L=4)			2	61.77
DVSCIFAR-10	[51]	STBP-tdBN	ResNet-19	10	67.80
	[29]	Dspike	ResNet-18	10	75.40
	[15]	MBPN	ResNet-19	10	74.40
	[14]	RMP-Loss	ResNet-19	10	76.20
	Ours (L=2)			2	80.70
		LM-HT	ResNet-18	4	81.00
	Ours (L=4)			2	81.90

surrogate gradients [29], learning function design [8, 14], energy-efficient training [13, 47, 34] and advanced neuron models [49, 43].

CIFAR-10 & CIFAR-100. For conventional static datasets, one can find that our solution demonstrates significant performance advantages. For ResNet-18 structure, we achieve the top-1 accuracies of 96.25% and 79.33% with merely 2 time-steps on CIFAR-10 and CIFAR-100 datasets, respectively. For ResNet-19 network with larger parameter scale, our method fulfills the precisions of 96.89% and 81.76% within 2 time-steps, which at least outperforms other corresponding works with 2.04% and 3.48% under the same time latency. In addition, it is worth noting that our above results have even exceeded the performance of other works with more time-steps (*e.g.* 6 steps).

ImageNet-200. For large-scale datasets, we also confirm the superiority of the LM-HT model. For a two-level LM-HT model, we achieve the accuracy of 61.04% within 2 time-steps, which is 4.47% higher than ASGL (4 steps) under the same-level time overhead. For a larger training time-step, one can note that our method will also demonstrate a significant advantage. For example, the two-level LM-HT model reaches the precision of 61.56% with 4 time-steps, which has surpassed ASGL (8 steps) with 4.75%.

DVSCIFAR-10. We also evaluate the effectiveness of our approach on neuromorphic datasets. Compared to other previous methods, our proposed model can achieve better results on shallower networks with fewer time-steps. For instance, the two-level LM-HT model can achieve the accuracy of 80.70% after merely 2 time-steps.

5.2 Performance Analysis of Hybrid Training

In our hybrid training framework, we first choose [2] as the backbone for our ANN-SNN Conversion stage. Subsequently, we replace the QCFS function layer by layer with the initialized LM-HT model and conduct STBP training for merely 30 epochs. Furthermore, we also consider other advanced conversion methods [16, 42] and multi-stage error correction method [17] as our comparative works.

Table 2: The performance of hybrid training based on the LM-HT model for CIFAR-100 dataset.

	Method	Architecture	ANN Acc.(%)	Time-steps	SNN Acc.(%)
[16]	RMP		71.22	128	63.76
[42]	SNM		74.13	32, 64, 128	71.80, 73.69, 73.95
[17]	SRP (+4 steps)		76.28	5, 6, 8	71.52, 74.31, 75.42
[2]	QCFS ($T_q=4$)		76.11	2, 4, 8	63.33, 69.70, 74.12
Ours	LM-HT (L=2)	VGG-16	-	2	75.97 (+6.27)
	LM-HT (L=4)			4	76.49 (+2.37)
	LM-HT (L=4)			2	76.38 (+2.26)
[2]	QCFS ($T_q=8$)		77.31	2, 4, 8	64.85, 70.50, 74.63
Ours	LM-HT (L=2)		-	2	76.31 (+5.81)
	LM-HT (L=2)			4	76.79 (+2.16)
	LM-HT (L=4)			2	76.08 (+1.45)
[16]	RMP		68.72	32, 64, 128	27.64, 46.91, 57.69
[17]	SRP (+4 steps)		69.94	5, 6, 8	46.48, 53.96, 59.34
[2]	QCFS ($T_q=4$)		63.90	2, 4, 8	38.04, 52.28, 61.77
Ours	LM-HT (L=2)	ResNet-20	-	2	63.55 (+11.27)
	LM-HT (L=4)			4	64.87 (+3.10)
	LM-HT (L=4)			2	63.43 (+1.66)
[2]	QCFS ($T_q=8$)		69.56	2, 4, 8	19.76, 34.17, 55.50
Ours	LM-HT (L=2)		-	2	67.08 (+32.91)
	LM-HT (L=2)			4	69.00 (+13.50)
	LM-HT (L=4)			2	67.21 (+11.71)

As shown in Table 2, after conducting the STBP fine-tuning optimization with relatively low computational overhead, we note that the performance of the converted SNNs under different quantization levels has been significantly improved and surpass other previous methods, especially under low time latency. For instance, compared to the ResNet-20 network after eight-level quantization (*i.e.* $T_q=8$), the two-level LM-HT model has achieved a performance improvement of 32.91% and 13.50% with 2 and 4 time-steps, respectively.

5.3 Impact of Different Threshold Level

We also investigate the impact of different threshold level settings on the performance of the LM-HT model. As we previously discussed, the output of an L -level LM-HT model at a single step is equivalent to the output sum of a vanilla IF model within L steps under the condition of inputting continuous uniform current. Therefore, for a given LT , the combination of larger L and smaller T corresponds to a higher uniform degree of the spike firing sequence and a more significant ANN-like learning attribute, while the configuration of smaller L and larger T will promote SNNs to capture more temporal information and dynamic features.

As shown in Table 1 and 2, we explore both cases $L = 2, T = 4$ and $L = 4, T = 2$, whose LT value all equals to 8. One can find that $L = 4, T = 2$ can achieve superior accuracy in the field of STBP direct training (61.77% v.s. 61.56%, 81.90% v.s. 81.00%), while $L = 2, T = 4$ reaches better results in terms of hybrid training (76.49% v.s. 76.38%, 76.79% v.s. 76.08%, 64.87% v.s. 63.43%, 69.00% v.s. 67.21%). This phenomenon indicates that a larger L can further enhance the learning performance of SNNs, while a larger T is conducive to a more reasonable gradient fine-tuning.

6 Conclusions

In this paper, we first investigate the mathematical equivalence among the multi-threshold model, vanilla spiking model and quantized ANNs, which promotes us to further tap the potential of the multi-threshold model in enhancing the learning performance of SNNs. Then we propose an advanced STBP training method based on the LM-HT model, which has been proven to cover the representation range of vanilla STBP and quantized ANNs training frameworks, thereby promoting SNNs to achieve performance at the same level as quantized ANNs while preserving the fundamental biological characteristics of spiking neurons simultaneously. Furthermore, from the perspective of mathematical expectation, the LM-HT model can fulfill lossless transformation from the traditional ANN-SNN Conversion framework under a specific parameter initialization condition. The brand-new hybrid

training method based on this principle can significantly alleviate the performance degradation of the converted SNNs under a few time-steps. Numerous experimental results have verified the superiority of our proposed method. We believe that our work will further promote in-depth research on advanced spiking neural model.

7 Impact Statements

This paper presents work whose goal is to advance the field of Machine Learning. There are many potential societal consequences of our work, none which we feel must be specifically highlighted here.

References

- [1] Léon Bottou. Stochastic gradient descent tricks. In *Neural networks: Tricks of the trade*, pages 421–436. Springer, 2012.
- [2] Tong Bu, Wei Fang, Jianhao Ding, PengLin Dai, Zhaofei Yu, and Tiejun Huang. Optimal ANN-SNN conversion for high-accuracy and ultra-low-latency spiking neural networks. In *International Conference on Learning Representations, 2022*.
- [3] Yongqiang Cao, Yang Chen, and Deepak Khosla. Spiking deep convolutional neural networks for energy-efficient object recognition. *International Journal of Computer Vision*, 113(1):54–66, 2015.
- [4] Ekin D Cubuk, Barret Zoph, Dandelion Mane, Vijay Vasudevan, and Quoc V Le. Autoaugment: Learning augmentation strategies from data. In *IEEE Conference on Computer Vision and Pattern Recognition*, pages 113–123, 2019.
- [5] Mike Davies, Narayan Srinivasa, Tsung-Han Lin, Gautham Chinya, Yongqiang Cao, Sri Harsha Choday, Georgios Dimou, Prasad Joshi, Nabil Imam, Shweta Jain, et al. Loihi: A neuromorphic manycore processor with on-chip learning. *IEEE Micro*, 38(1):82–99, 2018.
- [6] Jia Deng, Richard Socher, Lijia Li, Kai Li, and Feifei Li. Imagenet: A large-scale hierarchical image database. In *IEEE Conference on Computer Vision and Pattern Recognition*, 2009.
- [7] Shikuang Deng and Shi Gu. Optimal conversion of conventional artificial neural networks to spiking neural networks. In *International Conference on Learning Representations, 2021*.
- [8] Shikuang Deng, Yuhang Li, Shanghang Zhang, and Shi Gu. Temporal efficient training of spiking neural network via gradient re-weighting. *International Conference on Learning Representations, 2022*.
- [9] Terrance DeVries and Graham W Taylor. Improved regularization of convolutional neural networks with cutout. *arXiv preprint arXiv:1708.04552*, 2017.
- [10] Chaoteng Duan, Jianhao Ding, Shiyan Chen, Zhaofei Yu, and Tiejun Huang. Temporal effective batch normalization in spiking neural networks. In *Advances in Neural Information Processing Systems, 2022*.
- [11] Wei Fang, Zhaofei Yu, Yanqi Chen, Tiejun Huang, Timothée Masquelier, and Yonghong Tian. Deep residual learning in spiking neural networks. In *Advances in Neural Information Processing Systems, 2021*.
- [12] Wei Fang, Zhaofei Yu, Zhaokun Zhou, Ding Chen, Yanqi Chen, Zhengyu Ma, Timothée Masquelier, and Yonghong Tian. Parallel spiking neurons with high efficiency and ability to learn long-term dependencies. In *Advances in Neural Information Processing Systems, 2023*.
- [13] Isha Garg, Sayeed Shafayet Chowdhury, and Kaushik Roy. DCT-SNN: Using dct to distribute spatial information over time for learning low-latency spiking neural networks. *arXiv preprint arXiv:2010.01795*, 2020.
- [14] Yufei Guo, Xiaode Liu, Yuanpei Chen, Liwen Zhang, Weihang Peng, Yuhan Zhang, Xuhui Huang, and Zhe Ma. RMP-Loss: Regularizing membrane potential distribution for spiking neural networks. In *Proceedings of the IEEE/CVF International Conference on Computer Vision, 2023*.

- [15] Yufei Guo, Yuhan Zhang, Yuanpei Chen, Weihang Peng, Xiaode Liu, Liwen Zhang, Xuhui Huang, and Zhe Ma. Membrane potential batch normalization for spiking neural networks. In *Proceedings of the IEEE/CVF International Conference on Computer Vision*, 2023.
- [16] Bing Han, Gopalakrishnan Srinivasan, and Kaushik Roy. RMP-SNN: Residual membrane potential neuron for enabling deeper high-accuracy and low-latency spiking neural network. In *IEEE Conference on Computer Vision and Pattern Recognition*, pages 13558–13567, 2020.
- [17] Zecheng Hao, Tong Bu, Jianhao Ding, Tiejun Huang, and Zhaofei Yu. Reducing ann-snn conversion error through residual membrane potential. In *AAAI Conference on Artificial Intelligence*, 2023.
- [18] Zecheng Hao, Jianhao Ding, Tong Bu, Tiejun Huang, and Zhaofei Yu. Bridging the gap between anns and snns by calibrating offset spikes. In *International Conference on Learning Representations*, 2023.
- [19] Kaiming He, Xiangyu Zhang, Shaoqing Ren, and Jian Sun. Deep residual learning for image recognition. In *IEEE Conference on Computer Vision and Pattern Recognition*, pages 770–778, 2016.
- [20] Yifan Hu, Lei Deng, Yujie Wu, Man Yao, and Guoqi Li. Advancing spiking neural networks towards deep residual learning. *arXiv preprint arXiv:2112.08954*, 2021.
- [21] Saeed Reza Kheradpisheh and Timothée Masquelier. Temporal backpropagation for spiking neural networks with one spike per neuron. *International Journal of Neural Systems*, 30(06):2050027, 2020.
- [22] Seijoon Kim, Seongsik Park, Byungook Na, and Sungroh Yoon. Spiking-yolo: Spiking neural network for energy-efficient object detection. In *AAAI Conference on Artificial Intelligence*, 2020.
- [23] Alex Krizhevsky, Geoffrey Hinton, et al. Learning multiple layers of features from tiny images. 2009.
- [24] Yuxiang Lan, Yachao Zhang, Xu Ma, Yanyun Qu, and Yun Fu. Efficient converted spiking neural network for 3d and 2d classification. In *Proceedings of the IEEE/CVF International Conference on Computer Vision*, 2023.
- [25] Chen Li, Lei Ma, and Steve Furber. Quantization framework for fast spiking neural networks. *Frontiers in Neuroscience*, 16, 2022.
- [26] Hongmin Li, Hanchao Liu, Xiangyang Ji, Guoqi Li, and Luping Shi. Cifar10-dvs: an event-stream dataset for object classification. *Frontiers in Neuroscience*, 2017.
- [27] Yang Li and Yi Zeng. Efficient and accurate conversion of spiking neural network with burst spikes. In *International Joint Conference on Artificial Intelligence*, 2022.
- [28] Yuhang Li, Shikuang Deng, Xin Dong, Ruihao Gong, and Shi Gu. A free lunch from ANN: Towards efficient, accurate spiking neural networks calibration. In *International Conference on Machine Learning*, pages 6316–6325, 2021.
- [29] Yuhang Li, Yufei Guo, Shanghang Zhang, Shikuang Deng, Yongqing Hai, and Shi Gu. Differentiable spike: Rethinking gradient-descent for training spiking neural networks. In *Advances in Neural Information Processing Systems*, pages 23426–23439, 2021.
- [30] Ilya Loshchilov and Frank Hutter. Decoupled weight decay regularization. *arXiv preprint arXiv:1711.05101*, 2017.
- [31] Ilya Loshchilov and Frank Hutter. SGDR: stochastic gradient descent with warm restarts. In *International Conference on Learning Representations*, 2017.
- [32] Changze Lv, Jianhan Xu, and Xiaoqing Zheng. Spiking convolutional neural networks for text classification. In *International Conference on Learning Representations*, 2023.
- [33] Wolfgang Maass. Networks of spiking neurons: the third generation of neural network models. *Neural Networks*, 10(9):1659–1671, 1997.
- [34] Qingyan Meng, Mingqing Xiao, Shen Yan, Yisen Wang, Zhouchen Lin, and Zhiquan Luo. Towards memory and time-efficient backpropagation for training spiking neural networks. In *Proceedings of the IEEE/CVF International Conference on Computer Vision*, 2023.

- [35] Paul A Merolla, John V Arthur, Rodrigo Alvarez-Icaza, Andrew S Cassidy, Jun Sawada, Filipp Akopyan, Bryan L Jackson, Nabil Imam, Chen Guo, Yutaka Nakamura, et al. A million spiking-neuron integrated circuit with a scalable communication network and interface. *Science*, 345(6197):668–673, 2014.
- [36] Hesham Mostafa. Supervised learning based on temporal coding in spiking neural networks. *IEEE Transactions on Neural Networks and Learning Systems*, 29(7):3227–3235, 2017.
- [37] Jing Pei, Lei Deng, Sen Song, Mingguo Zhao, Youhui Zhang, Shuang Wu, Guanrui Wang, Zhe Zou, Zhenzhi Wu, Wei He, et al. Towards artificial general intelligence with hybrid tianjic chip architecture. *Nature*, 572(7767):106–111, 2019.
- [38] Nitin Rathi and Kaushik Roy. DIET-SNN: A low-latency spiking neural network with direct input encoding and leakage and threshold optimization. *IEEE Transactions on Neural Networks and Learning Systems*, pages 1–9, 2021.
- [39] Karen Simonyan and Andrew Zisserman. Very deep convolutional networks for large-scale image recognition. *arXiv preprint arXiv:1409.1556*, 2014.
- [40] Congyi Sun, Qinyu Chen, Yuxiang Fu, and Li Li. Deep spiking neural network with ternary spikes. In *IEEE Biomedical Circuits and Systems Conference (BioCAS)*, 2022.
- [41] Xiaoting Wang, Yanxiang Zhang, and Yongzhe Zhang. MT-SNN: Enhance spiking neural network with multiple thresholds. *arXiv preprint arXiv:2303.11127*, 2023.
- [42] Yuchen Wang, Malu Zhang, Yi Chen, and Hong Qu. Signed neuron with memory: Towards simple, accurate and high-efficient ANN-SNN conversion. In *International Joint Conference on Artificial Intelligence*, 2022.
- [43] Ziming Wang, Runhao Jiang, Shuang Lian, Rui Yan, and Huajin Tang. Adaptive smoothing gradient learning for spiking neural networks. In *International Conference on Machine Learning*, 2023.
- [44] Ziming Wang, Shuang Lian, Yuhao Zhang, Xiaoxin Cui, Rui Yan, and Huajin Tang. Towards lossless ANN-SNN conversion under ultra-low latency with dual-phase optimization. *arXiv preprint arXiv:2205.07473*, 2022.
- [45] Ziqing Wang, Yuetong Fang, Jiahang Cao, Qiang Zhang, Zhongrui Wang, and Renjing Xu. Masked spiking transformer. In *Proceedings of the IEEE/CVF International Conference on Computer Vision*, 2023.
- [46] Yujie Wu, Lei Deng, Guoqi Li, Jun Zhu, and Luping Shi. Spatio-temporal backpropagation for training high-performance spiking neural networks. *Frontiers in Neuroscience*, 12:331, 2018.
- [47] Qu Yang, Jibin Wu, Malu Zhang, Yansong Chua, Xinchao Wang, and Haizhou Li. Training spiking neural networks with local tandem learning. In *Advances in Neural Information Processing Systems*, 2022.
- [48] Man Yao, Jiakui Hu, Zhaokun Zhou, Yuan Li, Yonghong Tian, Bo Xu, and Guoqi Li. Spike-driven transformer. In *Proceedings of the IEEE/CVF International Conference on Computer Vision*, 2023.
- [49] Xingting Yao, Fanrong Li, Zitao Mo, and Jian Cheng. GLIF: A unified gated leaky integrate-and-fire neuron for spiking neural networks. In *Advances in Neural Information Processing Systems*, 2022.
- [50] Qiang Yu, Chenxiang Ma, Shiming Song, Gaoyan Zhang, Jianwu Dang, and Kay Chen Tan. Constructing accurate and efficient deep spiking neural networks with double-threshold and augmented schemes. *IEEE Transactions on Neural Networks and Learning Systems*, pages 1714–1726, 2022.
- [51] Hanle Zheng, Yujie Wu, Lei Deng, Yifan Hu, and Guoqi Li. Going deeper with directly-trained larger spiking neural networks. In *AAAI Conference on Artificial Intelligence*, pages 11062–11070, 2021.
- [52] Zhaokun Zhou, Yuesheng Zhu, Chao He, Yaowei Wang, Shuicheng Yan, Yonghong Tian, and Yuan Li. Spikformer: When spiking neural network meets transformer. In *International Conference on Learning Representations*, 2023.

A Proof of Theorem

A.1 Proof of Lemma 4.1 & Theorem 4.2

Before the proof of Theorem 4.2, we first need to introduce Lemma A.1:

Lemma A.1. Assume a continuous T -step input current $\mathbf{I}^l(1), \dots, \mathbf{I}^l(T)$, for a LM-HT model with L -level threshold, when $\forall t \in [1, T], \mathbf{I}^l(t) \in [0, L\theta^l)$ and $\mathbf{v}^l(0) \in [0, \theta^l), \lambda^l = 1$, we will have $\mathbf{v}^l(T) \in [0, \theta^l)$.

Proof. $\forall t \in [0, T)$, if $\mathbf{v}^l(t) \in [0, \theta^l)$, as $\mathbf{m}^l(t+1) = \mathbf{v}^l(t) + \mathbf{I}^l(t)$, we have $\mathbf{m}^l(t+1) \in [0, (L+1)\theta^l)$. Therefore, after the firing process $\mathbf{v}^l(t+1) = \mathbf{m}^l(t+1) - \mathbf{s}^l(t)\theta^l$, one can note that $\mathbf{v}^l(t+1) \in [0, \theta^l)$. According to the idea of mathematical induction, if we directly set $\mathbf{v}^l(0) \in [0, \theta^l)$, we can have $\mathbf{v}^l(T) \in [0, \theta^l)$. \square

Theorem 4.2. When $\lambda^l = 1, \mathbf{v}^l(0) \in [0, \theta^l)$, for a M-HT model with L -level threshold, after T time-steps, we will derive the following conclusions:

(i) If we further assume $\forall t \in [1, T], \mathbf{I}^l(t) \in [0, L\theta^l)$, we will have: $\forall t \in [1, T], \mathbf{s}^l(t) = \sum_{j=L(t-1)+1}^{Lt} \mathbf{s}_{IF}^l(j), \mathbf{v}^l(t) = \mathbf{v}_{IF}^l(Lt), \sum_{t=1}^T \mathbf{s}^l(t) = \sum_{j=1}^{LT} \mathbf{s}_{IF}^l(j)$.

(ii) If we further assume $\mathbf{I}^l(1) = \dots = \mathbf{I}^l(T)$, we will have: $\sum_{t=1}^T \mathbf{s}^l(t) = \text{clip} \left(\left\lfloor \frac{\mathbf{v}^l(0) + \sum_{t=1}^T \mathbf{I}^l(t)}{\theta^l} \right\rfloor, 0, LT \right)$.

Here the IF model has uniform input currents $\mathbf{I}^l(1)/L, \dots, \mathbf{I}^l(T)/L$ respectively within every L steps and satisfies $\mathbf{v}_{IF}^l(0) = \mathbf{v}^l(0)$.

Proof. (i) If we consider the pre-condition in Theorem 4.2 and combine Eq.(1) with (2), $\forall t \in [1, LT]$, we will have:

$$\mathbf{v}_{IF}^l(t) - \mathbf{v}_{IF}^l(t-1) = \mathbf{I}^l \left(\left\lfloor \frac{t}{L} \right\rfloor \right) / L - \mathbf{s}_{IF}^l(t)\theta^l. \quad (\text{S1})$$

Similarly, if we set $\lambda^l = 1$ and combine Eq.(8) with Eq.(9), $\forall t \in [1, T]$, we will have:

$$\mathbf{v}^l(t) - \mathbf{v}^l(t-1) = \mathbf{I}^l(t) - \mathbf{s}^l(t)\theta^l. \quad (\text{S2})$$

Then we accumulate Eq.(S1) along the time dimension and obtain the following equation:

$$\mathbf{v}_{IF}^l(Lt) - \mathbf{v}_{IF}^l(L(t-1)) = \mathbf{I}^l(t) - \sum_{j=L(t-1)+1}^{Lt} \mathbf{s}_{IF}^l(j)\theta^l. \quad (\text{S3})$$

As $\mathbf{I}^l(t) \in [0, L\theta^l)$, according to Lemma A.1, when $\mathbf{v}^l(t-1) = \mathbf{v}_{IF}^l(L(t-1)) \wedge \mathbf{v}^l(t-1) \in [0, \theta^l)$, we will have $\mathbf{v}^l(t) \in [0, \theta^l)$ and $\mathbf{v}_{IF}^l(Lt) \in [0, \theta^l)$. Considering $\mathbf{s}^l(t), \sum_{j=L(t-1)+1}^{Lt} \mathbf{s}_{IF}^l(j) \in \mathbb{N}$, if $\mathbf{s}^l(t) \neq \sum_{j=L(t-1)+1}^{Lt} \mathbf{s}_{IF}^l(j)$, one can note that $|\sum_{j=L(t-1)+1}^{Lt} \mathbf{s}_{IF}^l(j)\theta^l - \mathbf{s}^l(t)\theta^l| = |(\mathbf{v}^l(t) - \mathbf{v}^l(t-1)) - (\mathbf{v}_{IF}^l(Lt) - \mathbf{v}_{IF}^l(L(t-1)))| = |\mathbf{v}^l(t) - \mathbf{v}_{IF}^l(Lt)| \geq \theta^l$, which will violate the conclusion in Lemma A.1. Therefore, we can finally deduce that $\mathbf{s}^l(t) = \sum_{j=L(t-1)+1}^{Lt} \mathbf{s}_{IF}^l(j)$. Then we can further have $\mathbf{v}^l(t) = \mathbf{v}_{IF}^l(Lt)$ and $\sum_{t=1}^T \mathbf{s}^l(t) = \sum_{j=1}^{LT} \mathbf{s}_{IF}^l(j)$.

(ii) If we accumulate Eq.(S2) along the time dimension and divide θ^l on both sides, we will have the following equation:

$$\frac{\mathbf{v}^l(T) - \mathbf{v}^l(0)}{\theta^l} = \frac{\sum_{t=1}^T \mathbf{I}^l(t)}{\theta^l} - \sum_{t=1}^T \mathbf{s}^l(t). \quad (\text{S4})$$

If $\mathbf{I}^l(1) < 0$ or $\mathbf{I}^l(1) \geq L\theta^l$, it is obvious that we will have $\sum_{t=1}^T \mathbf{s}^l(t) = \text{clip} \left(\left\lfloor \frac{\mathbf{v}^l(0) + \sum_{t=1}^T \mathbf{I}^l(t)}{\theta^l} \right\rfloor, 0, LT \right) = 0$ or $\sum_{t=1}^T \mathbf{s}^l(t) = \text{clip} \left(\left\lfloor \frac{\mathbf{v}^l(0) + \sum_{t=1}^T \mathbf{I}^l(t)}{\theta^l} \right\rfloor, 0, LT \right) = L$. If $\mathbf{I}^l(1) \in [0, L\theta^l)$, according to Lemma A.1, we will have $\mathbf{v}^l(T) \in [0, \theta^l)$. As $\sum_{t=1}^T \mathbf{s}^l(t) \in$

\mathbb{N} , based on Eq.(S4), we can finally deduce that $\sum_{t=1}^T \mathbf{s}^l(t) = \frac{\mathbf{v}^l(0) + \sum_{t=1}^T \mathbf{I}^l(t)}{\theta^l} - \frac{\mathbf{v}^l(T)}{\theta^l} = \left\lfloor \frac{\mathbf{v}^l(0) + \sum_{t=1}^T \mathbf{I}^l(t)}{\theta^l} \right\rfloor = \text{clip} \left(\left\lfloor \frac{\mathbf{v}^l(0) + \sum_{t=1}^T \mathbf{I}^l(t)}{\theta^l} \right\rfloor, 0, LT \right)$.

One can note that Lemma 4.1 is actually a special case of Theorem 4.2 under the condition of $T = 1$, therefore Lemma 4.1 is also proven. \square

A.2 Proof of Corollary 4.3

Corollary 4.3. *If $\lambda^l = 1$, $\mathbf{v}^l(0) = 0$ and $\mathbf{I}^l(1) = \dots = \mathbf{I}^l(T)$, for a M-HT model with L-level threshold, $\mathbf{s}^l(1) = \dots = \mathbf{s}^l(T)$ is only satisfied when $\mathbf{I}^l(1) \in [k\theta^l, k\theta^l + \theta^l/T], \forall k = 0, \dots, L - 1$ or $\mathbf{I}^l(1) \in (-\infty, 0) \cup [L\theta^l, +\infty)$.*

Proof. If $\mathbf{I}^l(1) < 0$ or $\mathbf{I}^l(1) \geq L\theta^l$, it is obvious that we will have $\mathbf{s}^l(1) = \dots = \mathbf{s}^l(T) = 0$ or $\mathbf{s}^l(1) = \dots = \mathbf{s}^l(T) = L$. Otherwise, based on the conclusion $\sum_{t=1}^T \mathbf{s}^l(t) = \text{clip} \left(\left\lfloor \frac{\mathbf{v}^l(0) + \sum_{t=1}^T \mathbf{I}^l(t)}{\theta^l} \right\rfloor, 0, LT \right)$ in Theorem 4.2(ii), when $\mathbf{I}^l(1) \in [k\theta^l, k\theta^l + \theta^l/T], \forall k = 0, \dots, L - 1$, we will have $\sum_{t=1}^T \mathbf{s}^l(t) = kT, \forall k = 0, \dots, L - 1$. Note that $\forall T' \in [1, T]$, we can further have $\sum_{t=1}^{T'} \mathbf{s}^l(t) = kT', \forall k = 0, \dots, L - 1$. Therefore, it can be concluded that $\mathbf{s}^l(1) = \dots = \mathbf{s}^l(T) = k$. Instead, if $\mathbf{I}^l(1) \in [0, L\theta^l) \wedge \mathbf{I}^l(1) \notin [k\theta^l, k\theta^l + \theta^l/T], \forall k = 0, \dots, L - 1$, we will have $\sum_{t=1}^T \mathbf{s}^l(t) \neq kT, \forall k = 0, \dots, L - 1$. Therefore, $\mathbf{s}^l(1) = \dots = \mathbf{s}^l(T)$ does not hold true. \square

A.3 Proof of Theorem 4.4

Theorem 4.4. *When $\sum_{t=1}^T \mathbf{I}^l(t)/LT = \mathbf{W}^l \mathbf{r}_{IF}^{l-1}(T_q)$ and $\sum_{t=1}^T \mathbf{I}^l(t) \in [0, LT\theta^l]$, if $\forall i, j \in [1, T], \omega_{ij}^l = \frac{1}{T}$ and $\lambda^l = 1, \theta^l = \vartheta^l, \mathbf{v}^l(0) = \frac{\theta^l}{2}$, for L, T, T_q with arbitrary values, we have: $\mathbb{E} \left(\frac{\sum_{t=1}^T \mathbf{s}^l(t)\theta^l}{LT} - \frac{\vartheta^l}{T_q} \text{clip} \left(\left\lfloor \frac{\mathbf{W}^l \mathbf{r}_{IF}^{l-1}(T_q) T_q}{\vartheta^l} + \frac{1}{2} \right\rfloor, 0, T_q \right) \right) = 0$.*

Proof. If $\forall i, j \in [1, T], \omega_{ij}^l = \frac{1}{T}, \lambda^l = 1, \theta^l = \vartheta^l$ and $\mathbf{v}^l(0) = \frac{\theta^l}{2}$, combining with the conclusion mentioned in Theorem 4.2(ii), we will have $\frac{\sum_{t=1}^T \mathbf{s}^l(t)\theta^l}{LT} = \frac{\theta^l}{LT} \text{clip} \left(\left\lfloor \frac{\sum_{t=1}^T \mathbf{I}^l(t)}{\theta^l} + \frac{1}{2} \right\rfloor, 0, LT \right)$. According to the conclusion pointed out in [2], we have known that $\mathbb{E} \left(\frac{\theta^l}{LT} \text{clip} \left(\left\lfloor \frac{\mathbf{x}^l LT}{\theta^l} + \frac{1}{2} \right\rfloor, 0, LT \right) - \frac{\vartheta^l}{T_q} \text{clip} \left(\left\lfloor \frac{\mathbf{x}^l T_q}{\vartheta^l} + \frac{1}{2} \right\rfloor, 0, T_q \right) \right) = 0$, here $\mathbf{x}^l \in [0, \theta^l]$. Therefore, we directly set $\mathbf{x}^l = \sum_{t=1}^T \mathbf{I}^l(t)/LT = \mathbf{W}^l \mathbf{r}_{IF}^{l-1}(T_q)$ and then we will draw the final conclusion. \square

B Experimental Configuration

For static datasets, we attempt to suppress the possible overfitting phenomenon by utilizing data augmentation techniques including AutoAugment [4] and Cutout [9]. For DVSCIFAR-10 dataset, we resize each image to 48×48 pixels and split it into 10 frames. We respectively try to use SGD [1] and AdamW [30] as our optimizers. The corresponding initial learning rate and weight decay are set to $0.025, 5 \times 10^{-4}$ for SGD on CIFAR-10(100) and $0.02, 0.01$ for AdamW on DVSCIFAR-10. For ImageNet-200 dataset, we consider the optimal outcome between two options. Furthermore, in the hybrid training framework, our initial learning rate and weight decay are both set to 5×10^{-4} . For all experimental cases, we choose Cosine Annealing scheduler [31] to dynamically regulate the learning rate.

C The Pseudo-Code of Hybrid Training Algorithm

Algorithm 1 Hybrid training framework based on the LM-HT model.

Require: Pretrained QCFS ANN model $f_{\text{ANN}}(\mathbf{W}, T_q, \vartheta)$ with L_N layers; Dataset D ; Number of time-steps chosen for STBP training T .

Ensure: SNN model $f_{\text{SNN}}(\mathbf{W}, \mathbf{\Omega}, L, \lambda, \theta)$.

```

1: # Convert ANN to SNN
2: for  $l = 1$  to  $L_N$  do
3:    $f_{\text{SNN}} \cdot \mathbf{W}^l = f_{\text{ANN}} \cdot \mathbf{W}^l$ 
4:    $f_{\text{SNN}} \cdot \theta^l = f_{\text{ANN}} \cdot \vartheta^l$ 
5:    $f_{\text{SNN}} \cdot \mathbf{\Omega}^l = \frac{1}{T}$ 
6:    $f_{\text{SNN}} \cdot \lambda^l = 1$ 
7:    $f_{\text{SNN}} \cdot \mathbf{v}^l(0) = f_{\text{SNN}} \cdot \theta^l / 2$ 
8: end for
9: # STBP training based on the LM-H model
10: # Set  $f_{\text{SNN}} \cdot \mathbf{\Omega}^l, f_{\text{SNN}} \cdot \lambda^l$  as learnable parameters and  $f_{\text{SNN}} \cdot \theta^l$  as scalars
11: for (Image, Label) in  $D$  do
12:   for  $l = 1$  to  $L_N$  do
13:     if Is the first layer then
14:       for  $t = 1$  to  $T$  do
15:          $I^l(t) = I^l(t) \times L$ 
16:       end for
17:     end if
18:     LM-HT model performs forward propagation based on Eqs.(8)-(9) and Eqs.(11)-(12)
19:     LM-HT model performs back-propagation based on Eqs.(13)-(16)
20:   end for
21: end for
22: return  $f_{\text{SNN}}(\mathbf{W}, \mathbf{\Omega}, L, \lambda, \theta)$ 

```
